LANGMUIR

pubs.acs.org/Langmuir Article

Wetting Dynamics of a Lipid Monolayer

Shuo Guo,* Yong Jian Wang, Hsuan-Yi Chen, and Penger Tong

Cite This: *Langmuir* 2021, 37, 4879–4890 Read Online

ACCESS | Metrics & More | Article Recommendations

ABSTRACT: Direct measurement and control of the dynamic wetting properties of a lipid-coated water–air interface over a wide range of surface tension variations have many important applications. However, the wetting dynamics of the interface near its partial-to-complete wetting transition has not been fully understood. Here, we report a systematic study of the wetting dynamics of a lipid-coated water–air interface around a thin glass fiber of diameter 1–5 μm and length 100–300 μm. The glass fiber is glued onto the front end of a rectangular cantilever to form a "long-needle" atomic-force-microscope probe. Three surface modifications are applied to the glass fiber to change its wetting properties from hydrophilic to hydrophobic. A monolayer of phospholipid dipalmitoylphosphatidylcholine (DPPC) is deposited on the water–air interface in a homemade Langmuir–Blodgett trough, and the surface tension γ_L of the DPPC-coated water–air interface is varied in the range of $2.5 \lesssim \gamma_L \lesssim 72$ mN/m. From the measured hysteresis loop of the capillary force for the three coated fiber surfaces with varying γ_L, we observe a sharp transition from partial to complete wetting when γ_L is reduced to a critical value $(\gamma_L)_c$. The obtained values of $(\gamma_L)_c$ are 27 ± 1 mN/m for a DPPC-coated fiber surface and 23 ± 1 mN/m for an trichloro(1*H*,1*H*,2*H*,2*H*-perfluorooctyl) silane (FTS)-coated surface. Below $(\gamma_L)_c$, the contact angle θ_0 of the liquid interface is found to be zero for both hydrophobic fiber surfaces and the corresponding spreading parameter S becomes positive. For the FTS-coated fiber surface, the height of capillary rise exhibits a jump when γ_L is reduced to $(\gamma_L)_c$, which indicates that a rapidly advancing liquid film is formed on the fiber surface when the partial-to-complete wetting transition takes place. Our experiment thus establishes a quantitative method by which many other liquid interfaces coated with polymers, surfactants, and biomolecules (such as proteins and lipids) may be characterized dynamically.

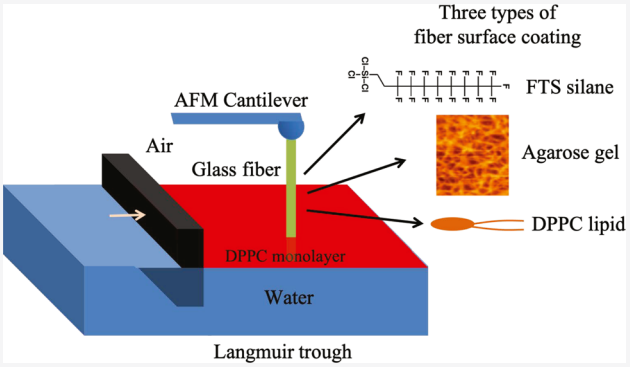

INTRODUCTION

Wetting of a liquid droplet on a solid surface is a common phenomenon in nature and technology, which is relevant to many practical applications ranging from spreading of droplets, lubricants, and coatings to microfluidic devices, drainage of liquids, and inkjet printing.[1−3] Wetting dynamics over an ambient solid surface is complicated and not well understood because it involves the motion of a contact line (CL) where a liquid interface between two (immiscible) fluids intersects with a solid surface. An outstanding problem associated with the CL is contact angle hysteresis (CAH), where the contact line is pinned by the physical roughness and/or chemical heterogeneities on the solid surface, which causes the dynamic contact angle between the liquid and solid surfaces to depend on the direction of fluid motion.[1,3−5] While considerable progress has been made recently in controlling the wettability of various textured solid surfaces[6−8] and in understanding the energetics associated with deformable soft substrates,[9−11] our understanding of CAH for ambient surfaces, which have real-world features such as irregular overlapping defects at different length scales, is still limited. Up to now, we do not have quantitative theoretical or experimental answers to simple questions such as how CAH is determined by the basic features of the substrate–fluid interactions.[1,5] The lack of experimental progress is partially due to the fact that direct observation of the contact angle in the immediate vicinity ($\lesssim$1 μm) of a moving CL is difficult with conventional optical methods.[12,13] As a result, most contact angle measurements were conducted in the region of 10–20 μm away from the core region of the moving contact line (MCL). The pinning of the CL at the microscopic level causes the CL dynamics to be very sensitive to the distance away from it, at which measurements are made.[1,4,5] These features make CAH a truly multiscale phenomenon. Direct measurements of CAH at the CL and

Received: January 11, 2021
Revised: March 31, 2021
Published: April 13, 2021

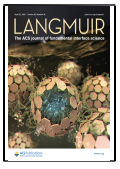

https://doi.org/10.1021/acs.langmuir.1c00079
Langmuir 2021, 37, 4879–4890

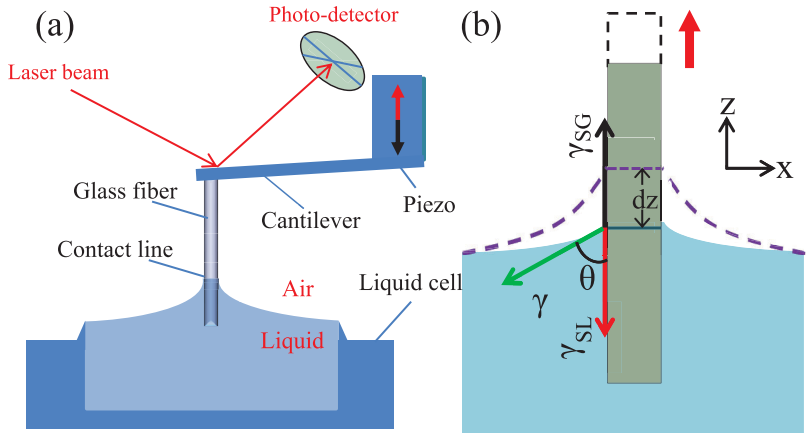

Figure 1. (a) Sketch of the AFM-based capillary force apparatus with a hanging fiber probe intersecting a liquid−air interface. (b) Three interfacial tensions acting at a three-phase contact line (dark blue line) formed on the fiber. Here, γ_{SG}, γ_{SL}, and γ are, respectively, the solid−gas, solid−liquid, and liquid−air interfacial tensions, and θ is the contact angle. The dashed lines indicate the changes of the meniscus of the liquid interface around the fiber when the fiber is pulled upward by a distance dz.

capillary force fluctuations are therefore needed to test different theoretical ideas.

The static contact angle θ, which is commonly used to characterize the wettability of a solid surface, is often measured by recording the cross-sectional images of a liquid droplet deposited on a solid surface under study. The value of θ is then obtained from the image analysis of the shape of the droplet. The experimental uncertainties of the measured θ using the imaging method are typically a few degrees. A refined protocol for performing reliable measurements of the advancing and receding contact angles of the probe droplet can reduce the error to 1°.[14] Recently, we developed a "long-needle" atomic-force-microscope (AFM) probe for the study of interfacial dynamics.[15−17] When the long-needle probe touches a liquid−air interface, a circular CL between the liquid interface and the needle surface is formed (see Figure 1a). As an accurate force sensor, the long-needle AFM can measure the capillary force acting on the CL at a high sampling rate (up to 1 MHz) and the corresponding contact angle θ between the liquid interface and the needle surface (see eq 4). With an accurate calibration, the long-needle AFM can measure the capillary force down to ∼10 pN, causing the determination of the contact angle θ to have an accuracy of ∼0.1°. Because it is made with a thin glass fiber, the long-needle probe provides a variety of opportunities for modifying the wetting properties of the fiber surface and changing its interactions with the liquid interface for the study of the CL dynamics over different solid substrates.[16,18−20] The long-needle AFM thus provides a versatile tool complementary to the conventional Wilhelmy plate method, which is often used for the study of interfacial wetting.[21]

In this work, we use a combined force apparatus of long-needle AFM with a homemade Langmuir−Blodgett trough to study how the wetting behavior of a lipid-coated water−air interface around a thin glass fiber changes with different surface coatings of the fiber and with varying surface tensions γ_L of the liquid interface. With the Langmuir−Blodgett trough, one can vary the surface coverage of a monolayer of phospholipid dipalmitoylphosphatidylcholine (DPPC) deposited on a water−air interface so that the liquid interfacial tension γ_L can be varied continuously from that for a pure water−air interface (∼72 mN/m) to a small value down to 2.5 mN/m.[22−25] At room temperature, the surface tension γ of simple liquids hardly goes below 20 mN/m, beyond which the liquids become highly volatile and are difficult to use in wetting experiments. With the large variation range of γ_L, we are able to introduce a transition from partial to complete wetting when γ_L is reduced to a critical value $(\gamma_L)_c$ so that the spreading parameter S (see eq 3) becomes positive.[3,26] With the long-needle AFM, we measure the equilibrium contact angle θ_0, the DPPC surface tension γ_{AFM}, and the capillary rise height h and study how these wetting properties change with γ_L before and after the wetting transition.

The remainder of the paper is organized as follows. We first present the working principle of the long-needle AFM and the experimental setup and sample preparation in Experiment section. The experimental results and discussions are presented in Results and Discussion section. Finally, the findings of this study are summarized in Conclusions section.

EXPERIMENT

AFM-Based Capillary Force Apparatus. Figure 1a shows the working principle of the AFM-based capillary force apparatus. A vertical glass fiber of diameter d in the range of 1−5 μm and length 100−300 μm is glued on the front end of a rectangular cantilever beam. The other end of the fiber is immersed through a liquid−air interface, at which a circular CL is formed on the fiber surface. With a close-loop piezoelectric stage, the fiber can be pulled upward and pushed downward through the liquid interface at a constant speed U.

As shown in Figure 1b, when the fiber is pulled upward by a distance dz, the work done to the fiber is $W = -f\,\mathrm{d}z = \pi d\,\mathrm{d}z(\gamma_{SG} - \gamma_{SL})$, where γ_{SG} and γ_{SL} are, respectively, the surface tensions of the solid−gas and solid−liquid interfaces. Therefore, the capillary force f acting on the fiber is

$$f = -\pi d(\gamma_{SG} - \gamma_{SL}) \tag{1}$$

At thermal equilibrium, a small amount of vapor molecules evaporated from the liquid interface adsorb on the fiber surface. In this case, one has $\gamma_{SG} = \gamma_{SV}$, where γ_{SV} is the solid−vapor interfacial tension. For a partially wetting liquid having a nonzero contact angle θ with the fiber surface, the Young−Dupré equation states are

$$\gamma_{SV} - \gamma_{SL} = \gamma\cos\theta \tag{2}$$

https://doi.org/10.1021/acs.langmuir.1c00079
Langmuir 2021, 37, 4879−4890

where γ is the surface tension of the liquid−air interface. In this case, the spreading parameter S, which is defined as

$$S = \gamma_{SG} - \gamma_{SL} - \gamma \tag{3}$$

becomes $S = \gamma(\cos\theta - 1) < 0$ for $\theta > 0$. Equation 1 then becomes

$$f = -\pi d\gamma \cos\theta, \ (\theta > 0) \tag{4}$$

where the sign of f is defined as $f \leq 0$ for $\theta \leq 90°$ and $f > 0$ for $\theta > 90°$.

In the experiment, we use AFM to accurately measure f with the cantilever either in stationary (static measurement) or at a constant speed U (dynamic measurement). Equation 4 is then used to determine the static contact angle θ when the values of d and γ are known. If the fiber surface is atomically smooth and chemically homogeneous, f is independent of the direction of U and the resulting θ takes the equilibrium value θ_0. For many ambient solid surfaces, however, the CL is often pinned by the physical roughness and/or chemical inhomogeneities on the surface, which causes the dynamic contact angle to depend on the direction of fluid motion.[3,4] In this case, θ takes two different values, with the advancing angle θ_a (when the fiber is pushed downward) being larger than the receding angle θ_r (when the fiber is pulled upward).[1,5−7]

The meniscus of the liquid interface around a stationary micron-sized fiber has the form[27]

$$r(z) = b \cosh\left[\frac{z}{b} - \ln\left(\frac{2l_c}{b}\right)\right] \tag{5}$$

where z is the height of the meniscus at the radial distance r, $l_c = \sqrt{\gamma/\rho g}$ is the capillary length, and $b = (d/2)\cos\theta$. Equation 5 was obtained under the two boundary conditions:[27] $\cot\theta_0 = dz(r)/dr$ at $r = d/2$ and $z \simeq 0$ at $r = l_c$. For a thin fiber with its diameter d (~2 μm) being much smaller than the capillary length l_c (~2 mm), the capillary force due to curvature is so dominant that gravity can be neglected when $x < l_c$. The capillary length l_c thus sets a natural cutoff length of the horizontal extent of the meniscus.

The height of capillary rise, $h \equiv z(r = d/2)$, on the fiber surface can be obtained by inverting eq 5 [16,28]

$$h \simeq \frac{d\cos\theta}{2} \ln\left[\frac{4l_c}{d(1 + \sin\theta)}\right] \tag{6}$$

For a liquid with $\gamma = 72$ mN/m, $\rho = 1 \times 10^3$ kg/m^3, $d = 2$ μm, and $\cos\theta = 1$, we have $l_c \simeq 2.7$ mm and $h \simeq 4.3d$.

Langmuir−Blodgett Trough Combined with a Long-Needle AFM. To measure the wetting dynamics of a lipid monolayer, we build a Langmuir−Blodgett trough, which is combined with the AFM-based capillary force apparatus. Figure 2a shows a sketch of the experimental setup. With the Langmuir−Blodgett trough, one is able to deposit a monolayer of lipid molecules on a water−air interface. A tightly fit moving barrier (black bar), which is placed on the left side of the trough, is used to vary the surface area occupied by the lipid monolayer. The surface tension γ_L of the lipid-coated interface is measured using a Wilhelmy plate force sensor, which is made of a piece of paper/platinum and is placed on the right side of the trough along with the AFM. The long-needle AFM shown in Figure 2 has several useful features for the study attempted here. (i) The hanging fiber used in this experiment has a diameter of 0.5−6 μm and a length of 100−300 μm. The overall dimension of the hanging fiber probe is designed so that one can ignore the buoyancy force acting on the fiber and have an easy operation in microassembly. The assembly method of the hanging fiber probe has been well developed and is described in ref 15. (ii) Glass fibers are used in the experiment, which are convenient for surface cleaning and treatment compared with other materials, such as metallic alloys.[29]

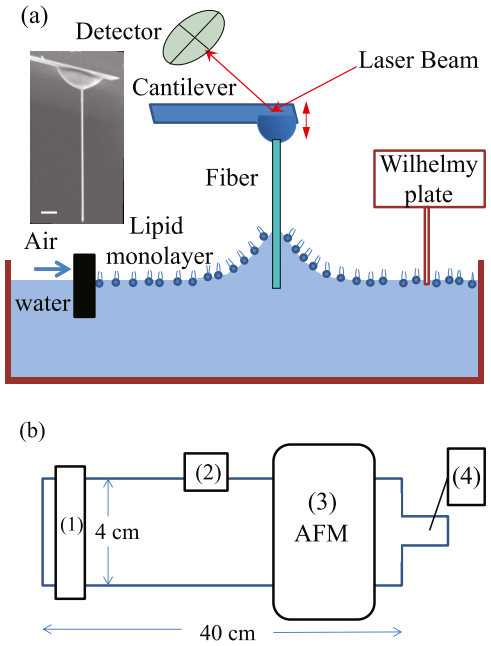

Figure 2. (a) Sketch of a homemade Langmuir−Blodgett trough combined with an AFM-based capillary force apparatus. A tightly fit moving barrier (black bar) is used to control the surface area occupied by a lipid monolayer, which is deposited on a water−air interface. The surface tension γ_L of the lipid-coated interface is measured using a Wilhelmy plate force sensor. The AFM hanging fiber probe intersects the water−air interface. The inset shows an scanning electron microscope (SEM) image of the glass hanging fiber probe with fiber diameter $d = 1.35$ μm. The scale bar is 10 μm. (b) Top view of the experimental setup. The Langmuir−Blodgett trough is mounted on a motor-controlled vertical moving stage (2), which can bring the lipid monolayer to the AFM hanging fiber probe. The moving barrier (1) is placed on the left side of the trough, and the AFM (3) and Wilhelmy plate force sensor (4) are placed on the right side of the trough. The dimensions of the trough are shown in the figure.

Preparation of the DPPC Monolayer. It is known that the wetting dynamics is extremely sensitive to the cleanliness of the solid surface.[3] In the experiment, great efforts are made to clean the entire system so that we can obtain accurate and reproducible results. Prior to each experiment, the trough and barrier are thoroughly cleaned with chloroform, ethanol, and then deionized water (obtained from a Barnstead three-column e-pure system at the resistivity of 18 MΩ·cm). The trough is then filled with deionized water. Next, 12.5 μL of a DPPC−chloroform solution (5 mg/mL, Avanti Polar Lipids) is injected onto the water−air interface with a syringe. All of the capillary measurements are conducted 15 min after the injection to ensure that the chloroform totally evaporates. Because DPPC is insoluble in water, the DPPC molecules form a lipid monolayer at the water−air interface. Using a Wilhelmy plate force sensor, we measure the surface pressure, $\pi \equiv 72.5$ mN/m $- \gamma_L$, as a function of area per molecule A, which is inversely proportional to the DPPC concentration.

https://doi.org/10.1021/acs.langmuir.1c00079
Langmuir 2021, 37, 4879−4890

Figure 3 shows a typical $\pi-A$ curve of the DPPC monolayer at T = 20 °C, which is obtained using our homemade

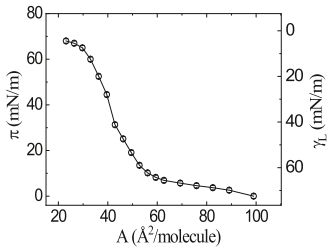

Figure 3. Measured surface pressure π (left axis) and the corresponding surface tension γ_L (right axis) as a function of area per molecule A (inversely proportional to the DPPC concentration) for a DPPC-coated water−air interface. The measurements are made at 20 °C using the homemade Langmuir−Blodgett trough with a monolayer compression speed of 5 mm/min. The solid line is drawn to guide the eye.

Langmuir−Blodgett trough. This $\pi-A$ curve is often used to characterize the phase behavior of lipid monolayers. The measured $\pi-A$ curve reveals two distinct features of the DPPC monolayer. First, the $\pi-A$ curve exhibits an abrupt rise at $A \simeq 60$ Å^2/molecule, which is caused by a structural transition of the DPPC monolayer from the liquid-expanded phase to the condensed phase.[24] Second, by further reducing the value of A to its low limit, $A \simeq 20$ Å^2/molecule, we find that the measured surface pressure π reaches its saturation value $\pi_S \simeq 70$ mN/m, suggesting that the surface tension of the DPPC monolayer reaches its low saturation value $(\gamma_L)_S \simeq 2.5$ mN/m at the high concentration limit. This low value of $(\gamma_L)_S$ is a unique feature of the DPPC monolayer[24] because the long saturated carbon chains in the DPPC monolayer can be tightly packed at a higher concentration limit. Thus, with the homemade Langmuir−Blodgett trough and the long-needle AFM, we are able to measure the wetting dynamics of the DPPC monolayer down to the low saturation value $(\gamma_L)_S$.

Operation of the Langmuir−Blodgett Trough and the Long-Needle AFM. After the deposition of the DPPC monolayer at the water−air interface, the long-needle AFM is placed on the top of the Langmuir−Blodgett trough with the hanging fiber probe not in contact with the liquid interface. The motor-controlled vertical moving stage (2), as shown in Figure 2b, is used to bring the DPPC monolayer to the hanging fiber probe. The distance between the fiber tip and the liquid−air interface is typically set at 10−15 μm. A z-axis piezo of the AFM with a traveling distance of 26 μm is then used to move the fiber up or down at a constant speed U. When the fiber tip touches the liquid interface, a large capillary force f is detected immediately by the AFM. As the fiber further moves downward, the circular CL sweeps over the fiber surface. When each set of the AFM measurements is completed, the liquid interface is moved 1 mm away from the fiber tip to ensure that the surface waves generated by moving the barrier do not contaminate the fiber probe. The DPPC concentration of the monolayer is varied by moving the barrier at a speed of 5 mm/min, which is slow enough to prevent any buckling of the DPPC monolayer.[24]

Surface Treatments of Glass Fiber. To change the wetting properties of the solid surface, the fiber glass surface is modified under three surface treatments. Before each treatment, the glass fiber is plasma-cleaned using a standard procedure.[19] It was found that the plasma-cleaned glass fiber has zero contact angle hysteresis in water and its peak-to-peak surface roughness is 0.8 nm over an area of 250 nm × 250 nm (see Figure 7 in ref 16).

In the first surface treatment, the glass fiber is coated with a thin layer of agarose gel of thickness ∼10 nm. The coating of agarose is conducted as follows. First, an aqueous solution of agarose is made by dissolving 0.3 wt % agarose powder (Sigma) in deionized water. The agarose solution is kept at the temperature T = 60 °C above its gelation temperature. Then, 100 μL of the agarose solution is transferred to a preheated rubber heating plate and forms a droplet on this hydrophobic surface. The droplet is kept at T = 60 °C during the coating process. Using a motor stage under a microscope, a plasma-cleaned glass fiber is dipped into the droplet, traveling downward for a distance of 50 μm, and is then pulled out. During the coating, the glass fiber moves slowly at a speed of 2 μm/s to ensure a smooth coating. This procedure is repeated five times, and then the fiber is left in air to dry out. Figure 4a

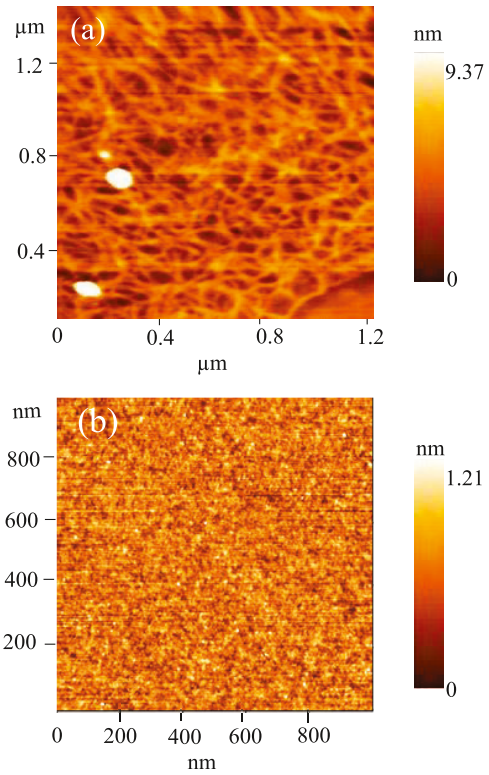

Figure 4. (a) AFM morphology image of an agarose-coated glass plate in air, which shows a network structure with a typical mesh size of ∼100 nm. A clear boundary between the thin layer of agarose and the bare glass surface is observed at the lower right corner of the image, revealing that the thickness of the agarose layer is approximately 10 nm. (b) AFM morphology image of an trichloro(1*H*,1*H*,2*H*,2*H*-perfluorooctyl) silane (FTS)-coated glass plate in air, which shows that the roughness of the FTS-coated surface in air is as low as ∼1.2 nm.

shows an AFM morphology image of an agarose-coated glass plate following the same coating procedure. The AFM image reveals that the agarose-coated surface in air has a network structure with a typical mesh size of ∼100 nm. The agarose-coated fiber is hydrophilic and water wets it completely with a zero contact angle (see the AFM measurements discussed below).

https://doi.org/10.1021/acs.langmuir.1c00079
Langmuir 2021, 37, 4879−4890

In the second surface treatment, the glass fiber is coated with a monolayer of DPPC. The coating is conducted using the homemade Langmuir−Blodgett trough, in which a DPPC monolayer is prepared as described above. The prepared DPPC monolayer is in the condensed phase with $\pi \geq 30$ mN/m. A plasma-cleaned glass fiber, which is already glued on the AFM cantilever, is dipped into the DPPC-coated water−air interface, traveling downward for a distance 50 μm, and is then pulled out. The advancing speed of the fiber is kept at 100 μm/s and the receding speed is 0.1 μm/s. The fast advancing and slow receding speeds reduce the possibility of forming a double layer of DPPC on the glass fiber. Under the conditions of having a high-density DPPC monolayer at the liquid interface and a slow receding of the fiber, we are able to coat the glass fiber with a uniform and densely packed monolayer of DPPC. The DPPC-coated fiber is then left open for complete evaporation of water on the fiber surface, and the remaining DPPC molecules are attached to the glass substrate by van der Waals forces. Because the plasma-cleaned glass surface is hydrophilic, the head group of the DPPC molecules adsorbs on the glass surface, leaving their hydrocarbon chains facing outward. As a result, the DPPC-coated fiber becomes hydrophobic with an advancing contact angle $\theta_a \simeq 84°$ in water (see Figure 8a for more details). Figure 8c in ref 30 shows an AFM scan of a DPPC-coated glass plate. The DPPC monolayer formed by Langmuir−Blodgett deposition was obtained under the same surface pressure as that used in this experiment. The rms surface roughness was found to be in the range of 0.8−1 nm.

In the third surface treatment, the glass fiber is coated with a monolayer of trichloro(1*H*,1*H*,2*H*,2*H*-perfluorooctyl) silane (FTS), which is covalently grafted onto the glass surface, following the procedures given in refs 31, 32. First, a plastic dish containing 50 μL of FTS (Aldrich) is placed in a vacuum chamber together with a plasma-cleaned glass fiber probe. The vacuum chamber is then sealed, and the pressure inside the chamber is set at 200 Torr. The vapor coating lasts for 30 min, and the sample is kept in the chamber for another 30 min after the pumping. The glass fiber probe is then flushed continuously with ethanol and water and dried in air.[33] Figure 4b shows an AFM morphology image of an FTS-coated glass plate following the same coating procedure. The AFM image reveals that the roughness of the FTS-coated surface in air is as low as ~1.2 nm. The FTS-coated fiber is hydrophobic with an advancing contact angle $\theta_a \simeq 100°$ in water (see Figure 8b for more details).

RESULTS AND DISCUSSION

Measurements of the Capillary Force Hysteresis Loop. *FTS-Coated Fiber.* Figure 5a shows how the measured f varies when an FTS-coated fiber is pushed downward (black advancing curve) and pulled upward (red receding curve) through a DPPC-coated water−air interface, whose surface tension is set at $\gamma_L \simeq 62.5$ mN/m. At $Z_i \simeq 12.9$ μm, the fiber touches the interface and a positive advancing capillary force ($f_a > 0$) is observed, indicating that the advancing contact angle θ_a for the FTS-coated fiber becomes larger than 90°. At $Z \simeq 26$ μm, the direction of fiber motion is reversed, and the red curve shows how the measured f changes in the receding direction. At $Z_f \simeq 6.4$ μm, the fiber detaches from the interface and the measured f goes back to zero. The black and red dashed lines in Figure 5a show, respectively, the average advancing capillary force $f_a \equiv -\pi d\gamma_L \cos\theta_a \simeq 52.0$ nN ($\theta_a \simeq 100.2°$) and the average receding capillary force $f_r \equiv -\pi d\gamma_L \cos\theta_r \simeq -70.5$ nN ($\theta_r \simeq 76.2°$).

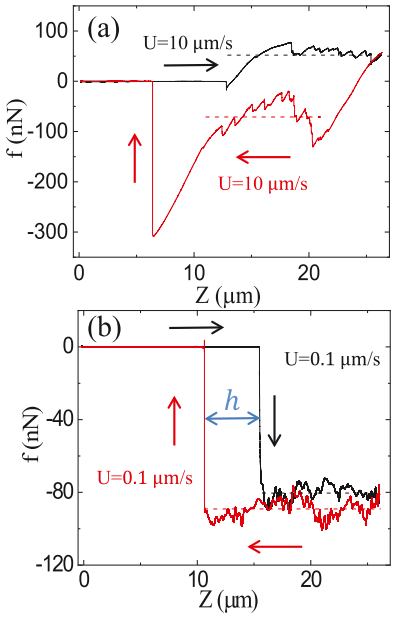

Figure 5. Variations of the measured capillary force f when an FTS-coated fiber of diameter $d = 1.5$ μm is pushed downward (black advancing (→) curve) and pulled upward (red receding (←) curve) through a DPPC-coated water−air interface. (a) The measurements are made with the surface tension $\gamma_L \simeq 62.5$ mN/m and the fiber moving speed $U = 10$ μm/s. The black and red dashed lines show, respectively, the average advancing capillary force $f_a \simeq 52.0$ nN ($\theta_a \simeq 100.2°$) and the receding capillary force $f_r \simeq -70.5$ nN ($\theta_r \simeq 76.2°$). (b) The measurements are made with the surface tension $\gamma_L = 5.7$ mN/m and the fiber moving speed $U = 0.1$ μm/s. The black and red dashed lines show, respectively, the average advancing capillary force $f_a \simeq -80.4$ nN and the receding capillary force $f_r \simeq -89.1$ nN. The distance h between the two vertical lines in the force loop indicates the capillary rise of the liquid interface on the fiber.

From the measured hysteresis loop shown in Figure 5a, we obtain three important quantities to characterize the wetting dynamics of the DPPC monolayer. The first quantity is the equilibrium contact angle θ_0, which is not known a priori. One often estimates θ_0 via the equation[16,34]

$$f_0 \simeq \frac{f_a + f_r}{2} \tag{7}$$

where $f_0 = -\pi d\gamma_L \cos\theta_0$ is the capillary force associated with the (unpinned) equilibrium state. From eq 7 we have

$$\cos\theta_0 \simeq \frac{\cos\theta_a + \cos\theta_r}{2} \tag{8}$$

where θ_a and θ_r are obtained from the AFM force measurement. In writing down eq 7, we have assumed that the system has a common reference state f_0 so that both the advancing and receding CLs can relax to it. In many practical circumstances, however, the CL is often pinned at an intermediate state and there is no reliable way to tell whether a CL has reached a true equilibrium contact angle θ_0 with its free energy at a global minimum.[20,33] Nevertheless, eq 8 allows us to use an experimentally well-defined measure to characterize the partial-to-complete wetting transition, as shown in Figure 8. In the discussions hereafter, we focus only on the

https://doi.org/10.1021/acs.langmuir.1c00079
Langmuir 2021, 37, 4879−4890

features that are not affected very much by the details of CL pinning.

The second quantity is the DPPC surface tension γ_{AFM}, which is obtained directly from the measured f at $\cos\theta = 1$ together with the known value of d [see eq 4]. As shown by the receding curve in Figure 5a, when the fiber reaches $Z_t \simeq 10.8$ μm (where the red dashed line ends), the fiber tip touches the liquid interface with a nonzero receding contact angle θ_r (because of capillary force hysteresis (CFH)). As the fiber moves further upward, because the CL is pinned at the edge of the fiber tip, the liquid interface is stretched while maintaining contact with the fiber tip and the dynamic contact angle θ decreases continuously, leading to a continuous and smooth increase in the measured f with no fluctuation, as seen in Figure 5a. Eventually, when the fiber reaches $Z_f \simeq 6.4$ μm, the value of θ becomes zero and the measured f reaches its maximum value, $f_m = \pi d\gamma_{AFM}$. At this point, the pinning force is no longer capable of balancing the restoring force of the stretched interface so that the fiber detaches from the liquid interface.

The third quantity is the height h of the capillary rise on the fiber surface. As shown in Figure 5a, the equilibrium height h associated with θ_r is $h = Z_i - Z_t \simeq 2.1$ μm. The dynamic height of the capillary rise for a detaching interface is $h_d = Z_i - Z_f \simeq 6.5$ μm. When the contact line pinning at the fiber tip is absent (i.e., when $\theta_a \simeq \theta_r \simeq 0$), the two definitions give the same result. In the following, we use $h = Z_i - Z_t$ to define the capillary rise for a given value of θ_r. In the next section, we discuss how the three wetting properties change with the concentration of the DPPC monolayer, which is characterized by its surface tension γ_L.

Figure 5b shows the measured hysteresis loop of f when the surface tension is changed to $\gamma_L = 5.7$ mN/m. The black and red dashed lines show, respectively, the average advancing capillary force $f_a \simeq -80.4$ nN and the receding capillary force $f_r \simeq -89.1$ nN. Compared with Figure 5a, we find that the capillary force hysteresis is small (i.e., $|f_a - f_r|/(|f_a + f_r|/2) \simeq 10\%$) and is comparable to capillary force fluctuations. It is also seen that just before the fiber detaches from the interface at $Z_f \simeq 10.2$ μm, the measured f_r remains approximately constant, contrary to that shown in Figure 5a. This result suggests that the DPPC-coated interface at $\gamma_L = 5.7$ mN/m already reaches the complete wetting state with $\theta_a \simeq \theta_r \simeq 0$. With eq 7, we find $f_0 = |f_a + f_r|/2 = \pi d\gamma_{AFM} = 84.75$ nN and the corresponding $\gamma_{AFM} \simeq 18.0$ mN/m. This value of γ_{AFM} is larger than the measured γ_L using the Wilhelmy plate. In Figure 9, we explain what causes this deviation. Figure 5 thus demonstrates that the wetting properties of the FTS-coated fiber depend sensitively on the surface tension γ_L of the DPPC monolayer. It is shown in Figure 8 that the FTS-coated fiber is partially wet by the DPPC-coated water−air interface at large values of γ_L and becomes completely wet at small values of γ_L. A partial-to-complete wetting transition is thus observed for the FTS-coated fiber intersecting a DPPC-coated water−air interface.

Agarose-Coated Fiber. Figure 6a shows a typical force loop obtained for an agarose-coated fiber when the surface tension is set at $\gamma_L = 55.4$ mN/m. When the fiber tip touches the interface at $Z_i \simeq 14.9$ μm, the measured f changes abruptly from $f = 0$ to $f \simeq -350$ nN. The negative sign indicates that the capillary force pulls the fiber into the liquid phase. As the fiber moves further downward, the advancing capillary force f_a remains approximately constant. At $Z \simeq 26$ μm, the direction of motion is reversed and the fiber moves upward at the same

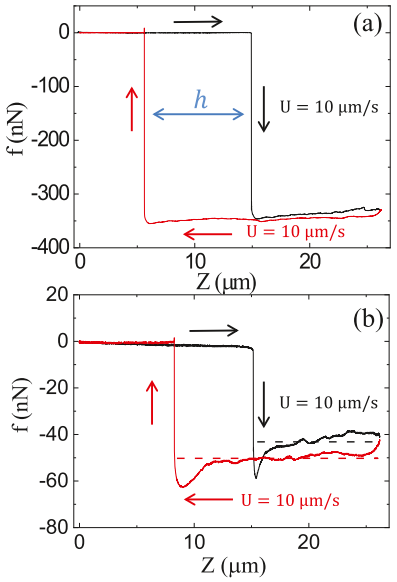

Figure 6. Variations of the measured capillary force f when an agarose-coated fiber is pushed downward (black advancing (→) curve) and pulled upward (red receding (←) curve) through a DPPC-coated water−air interface. (a) The measurements are made with the surface tension $\gamma_L \simeq 55.4$ mN/m, fiber diameter $d = 2$ μm, and fiber moving speed $U = 10$ μm/s. The distance h between the two vertical lines in the force loop indicates the capillary rise of the liquid interface on the fiber. (b) The measurements are made with $\gamma_L \simeq 13.6$ mN/m, $d = 1$ μm, and $U = 10$ μm/s. The black and red dashed lines show, respectively, the average advancing capillary force $f_a \simeq -42.7$ nN and the receding capillary force $f_r \simeq -50.4$ nN.

speed, as shown by the red curve. The receding capillary force f_r remains approximately constant and is very close to the advancing value, i.e., $f_a \simeq f_r$. At $Z_f \simeq 5.6$ μm, the fiber detaches from the liquid interface and no force is detected anymore. The distance between the two vertical lines in the force loop, $h = Z_i - Z_f \simeq 9.3$ μm as shown in Figure 6a, is caused by the capillary rise of the liquid interface on the fiber. This value of h agrees with the predicted value, $h \simeq 4.2d$, by eq 6 for $\theta = 0$.

In the experiment, the fiber diameter d is determined using a scanning electron microscope (SEM), as shown in the insets of Figures 2a and 10a, and the surface tension γ_L is determined using the Wilhelmy plate. The dynamic contact angle θ_a (or θ_r) is then obtained from the measured f_a (or f_r) using eq 4. For $\gamma_L = 55.4$ mN/m, we find from Figure 6a that the contact angles $\theta_r \simeq \theta_a \simeq 0$. No significant contact angle hysteresis is observed for the agarose-coated fiber at different surface tensions. Our results thus confirm that the agarose gel surface is wet completely by the DPPC-coated water−air interface.

Figure 6b shows the measured hysteresis loop of f at $\gamma_L = 13.6$ mN/m. The black and red dashed lines show, respectively, the average advancing capillary force $f_a \simeq -42.7$ nN and the receding capillary force $f_r \simeq -50.4$ nN. The obtained value of f_a agrees with the expected value of $f_a = -\pi d\gamma_L \cos\theta_a$ with $\theta_a = 0$. The obtained absolute value of f_r is close to but slightly larger than f_a. At this high DPPC concentration (low value of γ_L), we find that the measured value of f_r has a weak dependence on the fiber pulling speed U. This speed-dependent effect is not observed when the DPPC-coated monolayer is in the partial wetting regime ($\gamma_L > (\gamma_L)_c$). Because the capillary number, $Ca = \eta U/\gamma_L \simeq 0.7 \times 10^{-6}$, is very small for the DPPC-coated water−air interface with

https://doi.org/10.1021/acs.langmuir.1c00079
Langmuir 2021, 37, 4879−4890

viscosity η = 1 mPa·s, γ_L = 13.6 mN/m, and at U = 10 μm/s, this speed-dependent effect is not caused by the hydrodynamics. When the fiber is pulled too fast, it produces disturbances to the liquid interface, causing its surface tension to be larger than its equilibrium value γ_L. As a result, the obtained value of f_r has a small increase in amplitude. Because the focus of this work is on the equilibrium wetting properties of the lipid monolayer, we did not study the speed-dependent effect in detail.

DPPC-Coated Fiber. Figure 7a shows how the measured f varies when a DPPC-coated fiber is pushed downward (black advancing curve) and pulled upward (red receding curve) through a DPPC-coated water−air interface with $\gamma_L \simeq 62.6$ mN/m. At $Z_i \simeq 10.7$ μm, the fiber touches the interface, and at $Z \simeq 26$ μm, the direction of fiber motion is reversed. The fiber detaches from the interface and the measured f goes back to zero at $Z_f \simeq 2.8$ μm. From the measured hysteresis loop, we obtain $f_a \simeq 68.9$ nN ($\theta_a \simeq 98.1°$), $f_r \simeq -440$ nN ($\theta_r \simeq 26°$), and $\theta_0 = 40.9°$ (using eq 8). When the fiber reaches $Z_t \simeq 4.9$ μm (where the red dashed line ends), the fiber tip touches the liquid interface with a nonzero receding contact angle $\theta_r \simeq 26°$. The equilibrium height of the capillary rise associated with θ_r is $h = Z_i - Z_t \simeq 5.8$ μm. The dynamic height of the capillary rise for a detaching interface is $h_d = Z_i - Z_f \simeq 7.9$ μm.

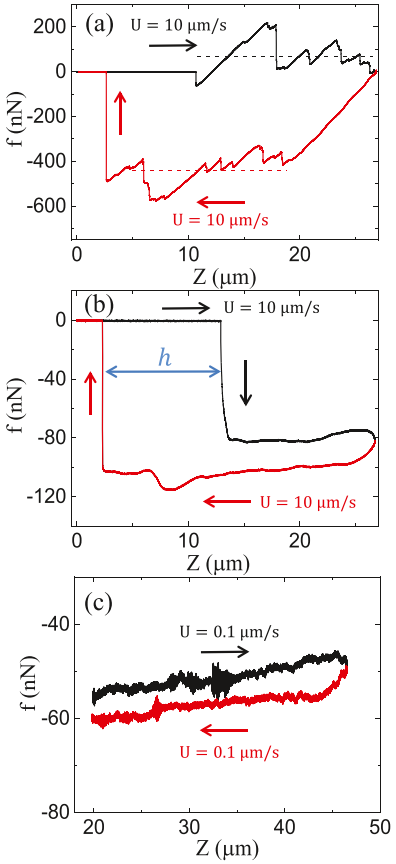

Figure 7. Variations of the measured capillary force f when a DPPC-coated fiber of d = 2.5 μm is pushed downward (black advancing (→) curve) and pulled upward (red receding (←) curve) through a DPPC-coated water−air interface. (a) The measurements are made with $\gamma_L \simeq 62.6$ mN/m and fiber speed U = 10 μm/s. The black and red dashed lines show, respectively, the average advancing capillary force $f_a \simeq 68.9$ nN ($\theta_a \simeq 98.1°$) and receding capillary force $f_r \simeq -440$ nN ($\theta_r \simeq 26°$). (b) The measurements are made with $\gamma_L \simeq 4.7$ mN/m and U = 10 μm/s. The average advancing capillary force $f_a \simeq -79.8$ nN and the receding capillary force $f_r \simeq -101.9$ nN. The distance h ($\simeq$10.8 μm) between the two vertical lines in the force loop indicates the capillary rise of the liquid interface on the fiber. (c) The measurements are made with $\gamma_L \simeq 4.7$ mN/m and U = 0.1 μm/s. The average advancing capillary force $f_a \simeq -51.2$ nN and receding capillary force $f_r \simeq -56.7$ nN.

Figure 7b shows the measured hysteresis loop of f when the surface tension is set at γ_L = 4.7 mN/m and the fiber moving speed is at U = 10 μm/s. From the measured hysteresis loop, we find $f_a \simeq -79.8$ nN and $f_r \simeq -101.9$ nN. The obtained values of f_a and f_b are larger than the maximum value, $f_m = -\pi d\gamma_L = -36.9$ nN, allowed for a DPPC monolayer at equilibrium with a contact angle θ = 0. It is seen that just before the fiber detaches from the interface at $Z_f \simeq 2.3$ μm, the measured f_r remains approximately constant, contrary to those shown in Figures 5a and 7a. This result suggests that the DPPC-coated interface at γ_L = 4.7 mN/m is already in the complete wetting regime with $\theta_a \simeq \theta_r \simeq 0$. The fact that the measured f_a (and f_r) is larger than f_m is not caused by the hydrodynamics but by some other dynamic effects. As mentioned above, for small values of γ_L, the measured f_r in Figure 6b exhibits a weak dependence on the fiber pulling speed U. This speed-dependent effect is also observed for the DPPC-coated fiber.

To minimize the speed-dependent effect, we reduce the fiber moving speed by 100 times to U = 0.1 μm/s. To further reduce perturbations to the DPPC-coated interface, we conduct capillary force measurements without taking the fiber in and out of the interface. Figure 7c shows the measured hysteresis loop of f when the moving fiber is kept inside the liquid during the entire scan. It is seen that for the same value of γ_L = 4.7 mN/m, the measured values of f_a and f_r at U = 0.1 μm/s are reduced by more than 35% when compared with those shown in Figure 7b, and they become very close to each other now. Using eq 7, we find $f_0 = |f_a + f_r|/2 = \pi d\gamma_{AFM} \simeq 54.0$ nN and the corresponding $\gamma_{AFM} \simeq 6.9$ mN/m. Within the experimental uncertainties of approximately ±1 mN/m, this value of γ_{AFM} is comparable to the expected value of γ_L = 4.7 mN/m (see more discussions on Figure 9b). Figure 7 thus demonstrates that the measured wetting properties at the low-speed limit of U = 0.1 μm/s are close to the equilibrium wetting properties of the DPPC-coated monolayer, which are the focus of this work. In the following, we present the results of three wetting properties as a function of γ_L, which are all obtained at the low-speed limit of U = 0.1 μm/s.

Measurements of the Equilibrium Contact Angle θ_0. As shown in eq 8, the value of θ_0 is determined from the capillary force measurements of $\cos\theta_a$ and $\cos\theta_r$ together with the known values of γ and d. For the agarose-coated fiber, we find $\theta_0 \simeq 0$ for the entire range of the DPPC surface tension ($2.5 < \gamma_L < 72.5$ mN/m).

Figure 8a shows the measured $\cos\theta_0$ as a function of γ_L for the DPPC-coated fibers with four different values of d. Because the DPPC coating is not very strong owing to its relatively weak adhesion to the glass fiber, the four sets of data for different fiber surfaces show some scatters. Nevertheless, the DPPC-coated fiber is stable enough so that the capillary force measurements by the AFM are reproducible for the same fiber surface, and the four sets of data for different DPPC-coated fibers collapse onto a common curve within the experimental uncertainties. This common curve shows a partial-to-complete wetting transition at a critical DPPC surface tension $(\gamma_L)_c$

https://doi.org/10.1021/acs.langmuir.1c00079
Langmuir 2021, 37, 4879−4890

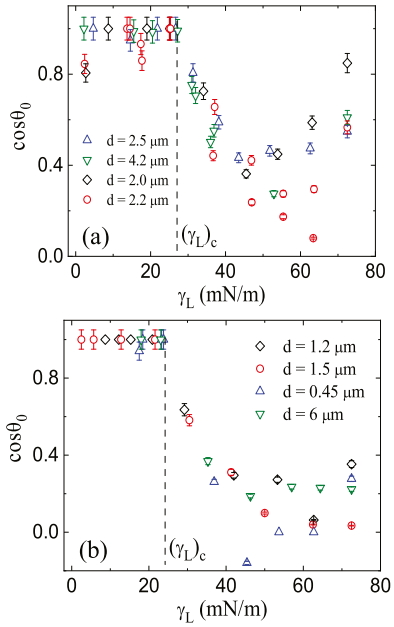

Figure 8. Measured $\cos\theta_0$ as a function of the DPPC surface tension γ_L for (a) the DPPC-coated fibers with four different fiber diameters d and (b) the FTS-coated fibers with four different values of d. The vertical dashed lines indicate the critical DPPC surface tension $(\gamma_L)_c$ at which a partial-to-complete wetting transition occurs. For the DPPC-coated fibers, we find $(\gamma_L)_c \simeq 27 \pm 1$ mN/m, and for the FTS-coated fibers, we have $(\gamma_L)_c \simeq 23 \pm 1$ mN/m.

($\simeq$27 mN/m as indicated by the vertical dashed line). When $\gamma_L < (\gamma_L)_c$, $\cos\theta_0 \simeq 1$ (i.e., $\theta_0 \simeq 0$) and thus the DPPC-coated fiber becomes completely wet. For $\gamma_L > (\gamma_L)_c$, the measured $\cos\theta_0$ continues to decrease with increasing γ_L and then situates at a value close to $\cos\theta_0 \simeq 0.3$ (i.e., $\theta_0 \simeq 72.5°$). For this contact angle, the DPPC-coated fiber is partially wet. It is seen that the partial-to-complete wetting transition is sharp and there is a distinct change in $\cos\theta_0$ when the transition takes place.

Figure 8b shows the measured $\cos\theta_0$ as a function of γ_L for the FTS-coated fibers with different values of d. The measured $\cos\theta_0$ shows a similar partial-to-complete wetting transition at $(\gamma_L)_c \simeq 23$ mN/m (vertical dashed line). For $\gamma_L > (\gamma_L)_c$, the measured $\cos\theta_0$ continues to decrease with increasing γ_L and then situate at a value close to $\cos\theta_0 \simeq 0.1$ (i.e., $\theta_0 \simeq 84.2°$). This value of θ_0 for the FTS-coated fiber is larger than that for the DPPC-coated fiber because the fluorinated carbon chains of the FTS are more hydrophobic compared with the hydrocarbon chains of DPPC. Also, because the FTS molecules are covalently grafted onto the glass surface, the FTS-coated fiber is more stable and the measured $\cos\theta_0$ shows fewer scatters.

The value of $(\gamma_L)_c$ quantifies how easily a solid surface can be wetted by a liquid. Our finding that the DPPC-coated surface has a larger value of $(\gamma_L)_c$ than the FTS-coated surface does is consistent with the previous experimental results obtained using pure liquid samples with different surface tensions γ.[26] Because the lowest value of γ for pure liquids at room temperature is about 20 mN/m, the critical surface tension γ_c obtained in previous experiments was actually the extrapolated value from the data in the partial wetting regime without reaching the complete wetting regime.[26] With the help of the DPPC monolayer, we are able to vary the surface tension over a wide range from 2.5 to 72 mN/m so that the measured $\cos\theta_0$ covers the entire range of the partial-to-complete wetting transition and no data extrapolation is needed. In this case, it is more accurate to determine the critical surface tension $(\gamma_L)_c$ as the upper boundary of the complete wetting regime, within which $\cos\theta_0 \simeq 1$. The experimental uncertainty of $(\gamma_L)_c$ is determined by the step size used to change the surface tension, which is 2 mN/m.

When a glass fiber is coated with a smooth and densely packed monolayer of DPPC or FTS molecules, its surface is noncharged and nonpolar and its disturbances to the hydrogen-bond network of water (bulk fluid) are minimal. In this case, the solid and liquid interactions are mainly of van der Waals type, and it was shown[27,35,36] that the partial-to-complete wetting transition occurs when the dielectric polarizability of the liquid becomes less than that of the solid, i.e., a liquid wets a solid surface completely if it is less polarizable than the solid. At the transition point, we have $(\gamma_L)_c \simeq \gamma_{SG}$, which is determined primarily by the dielectric polarizability of the solid.[3] Our finding that the DPPC-coated surface has a larger value of $(\gamma_L)_c$ than the FTS-coated surface suggests that the DPPC-coated surface is more polarizable (and hence more hydrophilic) compared with the FTS-coated surface. While the electronic polarizability of a single CF_3 group is about 20% larger than that of a single CH_3 group,[37] the packing density of fluorocarbons for an FTS-coated surface is approximately 40% smaller than that of hydrocarbons for a DPPC-coated surface.[36] As a result, the spatially averaged polarizability of an FTS-coated surface that a microscale contact line can feel is smaller than that of a DPPC-coated surface.

Measurements of the DPPC Surface Tension γ_{AFM} Using an AFM. For the agarose-coated fiber, we have shown above that $\theta_a \simeq \theta_r \simeq \theta_0 \simeq 0$ for all of the DPPC concentrations. Because no significant CFH is observed, both the advancing and receding capillary forces are used to obtain γ_{AFM} for better statistics. Figure 9a shows a comparison between the measured γ_{AFM} using five different agarose-coated fibers and the measured γ_L using a Wilhelmy plate made of a piece of paper. The five sets of data collapse onto a common curve, which is well described by the solid line $\gamma_{AFM} = \gamma_L$, within the experimental uncertainties.

Figure 9b shows a comparison between the measured γ_{AFM} using four different DPPC-coated fibers and γ_L. As shown in Figure 8a, when $\gamma_L < (\gamma_L)_c$ ($\simeq$27 mN/m), we have $\theta_a \simeq \theta_r \simeq \theta_0 \simeq 0$ and both the advancing and receding capillary forces are used to obtain γ_{AFM}. For $\gamma_L > (\gamma_L)_c$, we find the CFH with $f_a \neq f_r$. In this case, we use the maximum force, $f_m = \pi d\gamma_{AFM}$, measured in the receding direction before the fiber detaches from the liquid interface to obtain γ_{AFM}. Similar to Figure 9a, all of the data sets collapse onto a common curve, which is well described by the solid line $\gamma_{AFM} = \gamma_L$, within the experimental uncertainties.

Figure 9c shows a comparison between the measured γ_{AFM} using four different FTS-coated fibers and γ_L. The values of γ_{AFM} are determined in the same manner as that for the DPPC-coated fibers. It is seen that for $\gamma_L > (\gamma_L)_c$ ($\simeq$23 mN/m), all of the data sets are well described by the solid line $\gamma_{AFM} = \gamma_L$, within the experimental uncertainties. For $\gamma_L < (\gamma_L)_c$ (where $\theta_0 \simeq 0$), however, the measured γ_{AFM} shows systematic deviations from the solid line. This finding prompts us to re-examine eq 4, which is commonly used to relate the measured capillary force f with the contact angle θ. This equation is derived when the

https://doi.org/10.1021/acs.langmuir.1c00079
Langmuir 2021, 37, 4879−4890

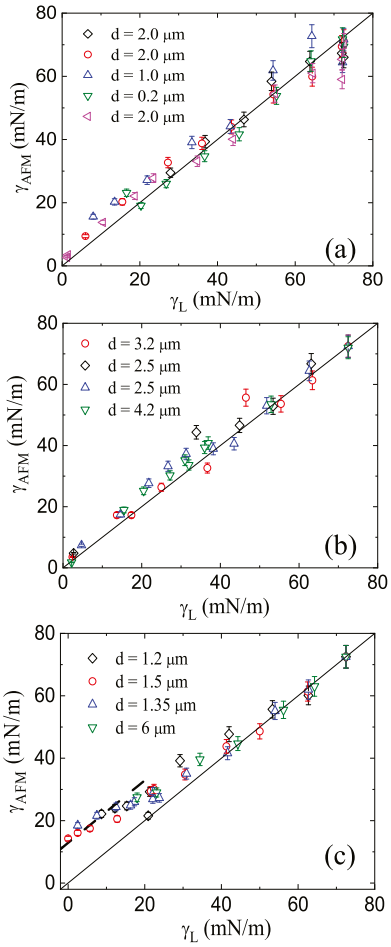

Figure 9. Comparison between the measured DPPC surface tensions by AFM (γ_{AFM}) and the Wilhelmy plate (γ_L). The measurements of γ_{AFM} are made with (a) five different agarose-coated fibers, (b) four different DPPC-coated fibers, and (c) four different FTS-coated fibers. The solid lines indicate $\gamma_{AFM} = \gamma_L$. The dashed line in (c) shows the linear function $\gamma_{AFM} = \gamma_L + 12.9$ mN/m.

fiber surface is in the partial wetting regime and the CL is at equilibrium with the three surface forces in balance, as shown in Figure 1b. In this case, the measured γ_{AFM} by AFM is the same as the measured γ_L by a Wilhelmy plate.

A special case arises when the liquid completely wets the fiber and correspondingly, $\theta_0 = 0$. In this case, the Young–Dupré equation shown in eq 2 may or may not apply, depending on whether or not the solid–air interface is truly at thermal equilibrium with the vapor phase.[1] For high-energy surfaces, such as the agarose-coated and DPPC-coated fiber surfaces and those used by Wilhelmy plates, a small amount of vapor molecules evaporated from the liquid interface can readily adsorb on them so that we have $\gamma_{SG} = \gamma_{SV}$ and $\gamma_{SG} - \gamma_{SL} = \gamma_L$ (or $S = \gamma_{SG} - \gamma_{SL} - \gamma_L = 0$). In this case, the CL is at equilibrium and eq 2 [or eq 4] still holds (with $\cos\theta = 1$). This explains our finding that $\gamma_{AFM} = \gamma_L$ in the complete wetting regime, as shown in Figure 9a,b.

Because the FTS-coated surface is more hydrophobic, water vapor molecules do not adsorb on it so that the FTS-coated surface is in a "dry" state (i.e., $\gamma_{SG} \neq \gamma_{SV}$)[27] and the three interfacial tensions are not balanced in the complete wetting regime (i.e., $\gamma_{SG} - \gamma_{SL} \neq \gamma_L$). In this case, the solid surface is not at thermal equilibrium with the vapor phase, and the system is in a dynamic spreading state with $S > 0$.[1] Consequently, eq 1, rather than eq 4, should be used to calculate f. With eq 1, we find $\gamma_{AFM} = \gamma_{SG} - \gamma_{SL}$. The results shown in Figure 9c confirm that the measured $\gamma_{AFM} = \gamma_{SG} - \gamma_{SL} > \gamma_L$ (or $S > 0$) in the complete wetting regime.

The measured γ_{AFM} at the small γ_L limit ($\gamma_L \ll (\gamma_L)_c$) can be described by a linear function $\gamma_{AFM} = \gamma_L + 12.9$ mN/m, as shown by the dashed line in Figure 9c. With $\gamma_{AFM} = \gamma_{SG} - \gamma_{SL}$ and eq 3, we find

$$\gamma_{AFM} = \gamma_L + S \tag{9}$$

The dashed line in Figure 9c is a plot of eq 9 with the intercept $S = 12.9$ mN/m. In the partial wetting regime ($S \leq 0$), one can use the Young–Dupré equation to determine the spreading parameter $S = \gamma_L(\cos\theta_0 - 1)$. In the complete wetting regime ($S > 0$), however, the Young–Dupré equation does not apply and the long-needle AFM provides a unique way to determine the value of S.

Measurements of the Capillary Rise h on the Fiber. As mentioned above, we obtain the height h of the capillary rise on the fiber surface from the measured distance $Z_i - Z_t$ for a given receding contact angle θ_r. Because the end surface of the fiber tip is not perfectly flat, the measured h is infected by a small amount of h_{cap}, which is generated by the residues on the fiber end surface resulting from imperfect cutting of the glass fiber tip. From the SEM image shown in the inset of Figure 10a, we find that the residues on the fiber end surface have a typical dimension of sub-micrometers and thus h_{cap} is of the same order.

Figure 10a shows the corrected capillary rise $(h - h_{cap})/d$ as a function of γ_L for an agarose-coated fiber. In the plot, the vertical axis is normalized by the fiber diameter d. The measured $(h - h_{cap})/d$ remains approximately constant over the entire range of the DPPC surface tension ($2.5 \lesssim \gamma_L \lesssim 72.5$ mN/m). For large values of γ_L ($\gtrsim$40 mN/m), the measured $(h - h_{cap})/d$ is close to (but slightly larger than) the theoretical prediction (dashed line), which is obtained using eq 6 with $\theta = 0°$. A larger deviation between the data and theory is observed for small values of γ_L ($\lesssim$25 mN/m).

Figure 10b shows the measured $(h - h_{cap})/d$ as a function of γ_L for four different DPPC-coated fibers. As mentioned above, the relatively larger scatters of the data at large values of γ_L are caused by the relatively weak adhesion of the DPPC molecules to the glass fiber. Nevertheless, the four sets of data for different DPPC-coated fibers collapse onto a common curve within the experimental uncertainties. From the measured receding capillary force f_r, we find the corresponding receding contact angle $\theta_r \simeq 45°$ for all of the DPPC-coated fibers used. For large values of γ_L ($\gtrsim$40 mN/m), the measured $(h - h_{cap})/d$ remains approximately constant and is close to the theoretical prediction (solid line), which is obtained using eq 6 with $\theta = 45°$. For small values of γ_L ($\lesssim$25 mN/m), the measured $(h - h_{cap})/d$ starts to increase with decreasing γ_L and reaches a maximum value of ~4.5 at the low γ_L limit ($\simeq$2.5 mN/m).

Figure 10c shows the measured $(h - h_{cap})/d$ as a function of γ_L for two different FTS-coated fibers. While they were prepared with the same coating protocol, the two FTS-coated fibers exhibit somewhat different wetting properties. From the measured receding capillary force f_r, we find that the $d = 1.2$ μm fiber (black diamonds) has a receding contact angle $\theta_r \simeq 60°$ whereas the $d = 1.5$ μm fiber (red circles) has $\theta_r \simeq 71°$. We believe that this difference in θ_r reflects the difference in the

https://doi.org/10.1021/acs.langmuir.1c00079
Langmuir 2021, 37, 4879–4890

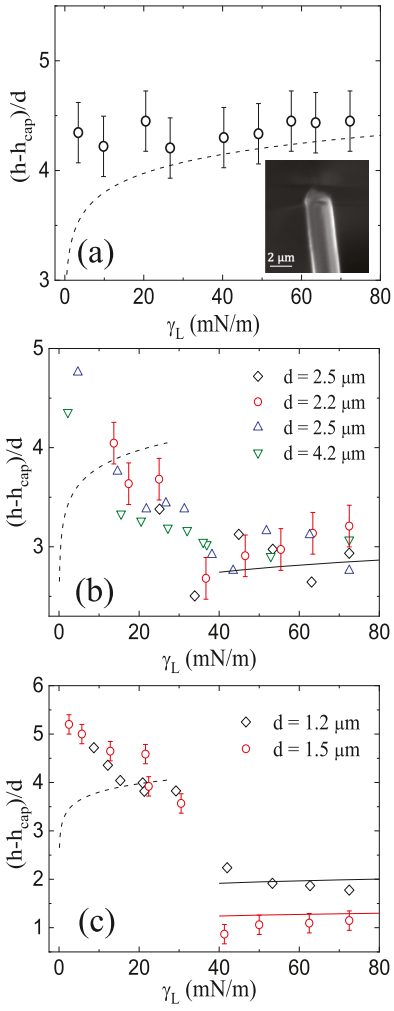

Figure 10. Measured capillary rise $(h - h_{cap})/d$ as a function of the DPPC surface tension γ_L. The vertical axis is normalized by the fiber diameter d. (a) Measurements made with an agarose-coated fiber. The inset shows a magnified SEM image of the hanging fiber tip. (b) Measurements made with four different DPPC-coated fibers. (c) Measurements made with two different FTS-coated fibers. The dashed lines show the plots of eq 6 with $\theta = 0°$. The solid lines show the plots of eq 6 with (b) $\theta = 45°$ and (c) $\theta = 60°$ (black solid line) and $\theta = 71°$ (red solid line), respectively (see the text for more explanations).

microscopic details of the defect landscape between the two fibers, which cannot be precisely controlled by the surface coating procedure. For $\gamma_L \gtrsim 40$ mN/m, the measured values of $(h - h_{cap})/d$ remain approximately constant and agree with the theoretical predictions (black and red solid lines), which are obtained using eq 6 with $\theta = 60°$ and $\theta = 71°$, respectively. For $\gamma_L \lesssim 25$ mN/m, the measured $(h - h_{cap})/d$ increases with decreasing γ_L and reaches a maximum value of ~5.2 at the low γ_L limit ($\simeq$2.5 mN/m).

Figure 10 thus demonstrates that for large values of γ_L ($\gtrsim$40 mN/m), the measured $(h - h_{cap})/d$ with different receding contact angles θ_r can all be explained satisfactorily with eq 6. For small values of γ_L ($\lesssim$25 mN/m), a transition from partial to complete wetting takes place and the contact angle becomes zero ($\theta = 0°$). In this case, the measured $(h - h_{cap})/d$ does not follow the theoretical predictions (dashed lines), which are obtained using eq 6 with $\theta = 0°$. The measured $(h - h_{cap})/d$ shows an opposite trend compared with the theoretical prediction, which decreases sharply as $\gamma_L \to 0$. Therefore, it is necessary to re-examine the conditions under which eq 6 is obtained.

First, eq 6 is derived by assuming that surface tension completely determines the shape of the liquid−air interface, and the effect of gravity only appears as a cutoff length, at which the rise of the liquid surface approaches zero. Therefore, the deviation of eq 6 from the measured $(h - h_{cap})/d$ as $\gamma_L \to 0$ shown in Figure 10a simply reflects the fact that one should properly include the effect of gravity when needed. Second, if wetting transition occurs when the surface tension of the liquid drops below some critical value $(\gamma_L)_c$, the liquid spreads on the fiber surface by climbing up and forming a liquid film. As this film advances, its thickness also gradually evolves to some thickness, which is determined by the disjoining pressure.[27] Figure 10b shows that for a liquid with $S \simeq 0$, the capillary rise gradually increases as γ_L crosses $(\gamma_L)_c$ due to the slow motion of the liquid film during the measurement. On the other hand, Figure 10c shows that for $S > 0$, there is a jump in the capillary rise as γ_L crosses $(\gamma_L)_c$, indicating a rapid advancing liquid film formed on the fiber surface.

■ CONCLUSIONS

We have developed a combined force apparatus of long-needle AFM with a homemade Langmuir−Blodgett trough, which is equipped with a Wilhelmy plate for independent measurement of the surface tension of a water−air interface coated with a monolayer of phospholipid DPPC. The long-needle AFM probe is made with a thin glass fiber, which is suitable for a variety of surface treatments. Three surface modifications are employed in the experiment. First, the glass fiber is coated with a thin layer of agarose gel, which is a hydrophilic surface covered by a thin layer of water. Second, the fiber surface is coated with a monolayer of DPPC with (hydrophobic) hydrocarbon chains facing outward. Third, the fiber surface is coated with a monolayer of FTS with (highly hydrophobic) fluorocarbon chains facing outward. The Langmuir−Blodgett trough together with the Wilhelmy plate allows us to vary and monitor in real time the surface tension γ_L of the DPPC-coated water−air interface over a wide range from that for a pure water−air interface (~72 mN/m) to a small value down to 2.5 mN/m. This system thus provides a large parameter space for the study of wetting dynamics with different solid−liquid interactions.

With this combined force apparatus, we systematically studied the wetting dynamics of a DPPC-coated water−air interface around a thin glass fiber with three different surface coatings. By varying the surface tension γ_L of the liquid interface, we observed a transition from partial to complete wetting when γ_L is reduced to a critical value $(\gamma_L)_c$. Below $(\gamma_L)_c$, we find that the contact angle θ_0 between the liquid interface and the DPPC-coated as well as FTS-coated fiber surfaces becomes zero and consequently the spreading parameter S given in eq 3 becomes positive. The value of $(\gamma_L)_c$ quantifies how easily a solid surface can be wetted by a liquid, and we find that the DPPC-coated surface has a larger value of $(\gamma_L)_c$ than the FTS-coated surface does. In the complete wetting regime, the measured maximum capillary force per unit length, γ_{AFM}, is no longer equal to the equilibrium surface tension γ_L, as measured by the Wilhelmy plate, and the difference between the two quantities provides a direct measure of the spreading parameter S. For the FTS-coated fiber, we find $S \simeq 12.9$ mN/m and its capillary rise

https://doi.org/10.1021/acs.langmuir.1c00079
Langmuir 2021, 37, 4879−4890

height h exhibits a jump when γ_L is reduced to $(\gamma_L)_c$. This jump suggests that a rapidly advancing liquid film is formed on the fiber surface when the partial-to-complete wetting transition takes place. Our experiment thus establishes a quantitative method by which many other liquid interfaces coated with polymers, surfactants, and biomolecules (such as proteins and lipids) may be characterized dynamically.

AUTHOR INFORMATION

Corresponding Author

Shuo Guo − *School of Physical Science and Technology, ShanghaiTech University, Shanghai 201210, China;* orcid.org/0000-0001-7239-9207; Email: guoshuo@shanghaitech.edu.cn

Authors

Yong Jian Wang − *Department of Physics, Hong Kong University of Science and Technology, Kowloon, Hong Kong, China*

Hsuan-Yi Chen − *Department of Physics and Center for Complex Systems, National Central University, Taoyuan City 32001, Taiwan; Institute of Physics, Academia Sinica, Taipei 11529, Taiwan*

Penger Tong − *Department of Physics, Hong Kong University of Science and Technology, Kowloon, Hong Kong, China*

Complete contact information is available at: https://pubs.acs.org/10.1021/acs.langmuir.1c00079

Notes

The authors declare no competing financial interest.

ACKNOWLEDGMENTS

This work was supported in part by the startup support of ShanghaiTech University (S.G.), Shanghai Pujiang Program under grant no. 19PJ1407800 (S.G.), and NSF of China under grant no. 32071253 (S.G.), by RGC of Hong Kong under grant nos. 16301719 (P.T.) and 16300920 (P.T.), and by MoST of Taiwan under grant no. 108-2112-M-008-016 (H.-Y.C.). H.-Y.C. also acknowledges support by NCTS of Taiwan.

REFERENCES

(1) Bonn, D.; Eggers, J.; Indekeu, J.; Meunier, J.; Rolley, E. Wetting and Spreading. *Rev. Mod. Phys.* **2009**, *81*, No. 739.

(2) Snoeijer, J. H.; Andreotti, B. Moving Contact Lines: Scales, Regimes, and Dynamical Transitions. *Annu. Rev. Fluid Mech.* **2013**, *45*, 269−292.

(3) de Gennes, P.-G. Wetting: statics and dynamics. *Rev. Mod. Phys.* **1985**, *57*, No. 827.

(4) Leger, L.; Joanny, J.-F. Liquid spreading. *Rep. Prog. Phys.* **1992**, *55*, No. 431.

(5) Decker, E. L.; Garoff, S. Contact angle hysteresis: The need for new theoretical and experimental models. *J. Adhes.* **1997**, *63*, 159−185.

(6) Quéré, D. Wetting and roughness. *Annu. Rev. Mater. Res.* **2008**, *38*, 71−99.

(7) Ramiasa, M.; Ralston, J.; Fetzer, R.; Sedev, R. The influence of topography on dynamic wetting. *Adv. Colloid Interface Sci.* **2014**, *206*, No. 275.

(8) Farshchi-Tabrizi, M.; Kappl, M.; Cheng, Y.; Gutmann, J.; Butt, H.-J. On the Adhesion between Fine Particles and Nanocontacts: An Atomic Force Microscope Study. *Langmuir* **2006**, *22*, 2171−2184.

(9) Jerison, E. R.; Xu, Y.; Wilen, L. A.; Dufresne, E. R. Deformation of an Elastic Substrate by a Three-Phase Contact Line. *Phys. Rev. Lett.* **2011**, *106*, No. 186103.

(10) Marchand, A.; Das, S.; Snoeijer, J. H.; Andreotti, B. Contact Angles on a Soft Solid: From Young's Law to Neumann's Law. *Phys. Rev. Lett.* **2012**, *109*, No. 236101.

(11) Style, R. W.; Boltyanskiy, R.; Che, Y.; Wettlaufer, J. S.; Wilen, L. A.; Dufresne, E. R. Universal Deformation of Soft Substrates Near a Contact Line and the Direct Measurement of Solid Surface Stresses. *Phys. Rev. Lett.* **2013**, *110*, No. 066103.

(12) Marsh, J. A.; Garoff, S.; Dussan, E. B. V. Dynamic contact angles and hydrodynamics near a moving contact line. *Phys. Rev. Lett.* **1993**, *70*, No. 2778.

(13) Chen, Q.; Ramé, E.; Garoff, S. The velocity field near moving contact lines. *J. Fluid Mech.* **1997**, *337*, 49.

(14) Huhtamäki, T.; Tian, X.; Korhonen, J. T.; Ras, R. H. A. Surface-wetting characterization using contact-angle measurements. *Nat. Protoc.* **2018**, *13*, 1521−1538.

(15) Xiong, X.-M.; Guo, S.; Xu, Z.-L.; Sheng, P.; Tong, P. Development of an atomic-force-microscope-based hanging-fiber rheometer for interfacial microrheology. *Phys. Rev. E* **2009**, *80*, No. 061604.

(16) Wang, Y. J.; Guo, S.; Chen, H.-Y.; Tong, P. Understanding contact angle hysteresis on an ambient solid surface. *Phys. Rev. E* **2016**, *93*, No. 052802.

(17) Guo, S.; Xiong, X.-M.; Xu, Z.-L.; Sheng, P.; Tong, P. Measurement of the friction coefficient of a fluctuating contact line using an AFM-based dual-mode mechanical resonator. *Chin. Phys. B* **2014**, *23*, No. 116802.

(18) Guo, S.; Gao, M.; Xiong, X.-M.; Wang, Y. J.; Wang, X.-P.; Sheng, P.; Tong, P. Direct Measurement of Friction of a Fluctuating Contact Line. *Phys. Rev. Lett.* **2013**, *111*, No. 026101.

(19) Guo, S.; Lee, C. H.; Sheng, P.; Tong, P. Measurement of contact-line dissipation in a nanometer-thin soap film. *Phys. Rev. E* **2015**, *91*, No. 012404.

(20) Guan, D. S.; Wang, Y. J.; Charlaix, E.; Tong, P. Asymmetric and Speed-Dependent Capillary Force Hysteresis and Relaxation of a Suddenly Stopped Moving Contact Line. *Phys. Rev. Lett.* **2016**, *116*, No. 066102.

(21) Eriksson, L. G. T.; Claesson, P. M.; Eriksson, J. C.; Yaminsky, V. V. Equilibrium Wetting Studies of Cationic Surfactant Adsorption on Mica: 1. Mono- and Bilayer Adsorption of CTAB. *J. Colloid Interface Sci.* **1996**, *181*, 476−489.

(22) McConnell, H. M. Structures and Transitions in Lipid Monolayers at the Air-Water Interface. *Annu. Rev. Phys. Chem.* **1991**, *42*, 171−195.

(23) Knobler, C. M.; Desai, R. Phase Transitions in Monolayers. *Annu. Rev. Phys. Chem.* **1992**, *43*, 207−236.

(24) Lee, K. Y. Collapse Mechanisms of Langmuir Monolayers. *Annu. Rev. Phys. Chem.* **2008**, *59*, No. 771.

(25) Choi, S. Q.; Steltenkamp, S.; Zasadzinski, J. A.; Squires, T. M. Active microrheology and simultaneous visualization of sheared phospholipid monolayers. *Nat. Commun.* **2011**, *2*, No. 312.

(26) Zisman, W. A. Relation of the Equilibrium Contact Angle to Liquid and Solid Constitution. *Adv. Chem.* **1964**, *43*, 1−51.

(27) de Gennes, P.-G.; Brochard-Wyart, F.; Quéré, D. *Capillarity and Wetting Phenomena*; Springer: New York, USA, 2004; p 89.

(28) Guo, S.; Xu, X.; Qian, T.; Di, Y.; Doi, M.; Tong, P. Onset of thin film meniscus along a fibre. *J. Fluid Mech.* **2019**, *865*, 650−680.

(29) Dupré de Baubigny, J.; Benzaquen, M.; Fabie, L.; Delmas, M.; Aime, J.-P.; Legros, M.; Ondarcuhu, T. Shape and Effective Spring Constant of Liquid Interfaces Probed at the Nanometer Scale: Finite Size Effects. *Langmuir* **2015**, *31*, 9790−9798.

(30) Kurniawan, J.; de Souza, J. F. V.; Dang, A. T.; Liu, G.-Y.; Kuhl, T. L. Preparation and Characterization of Solid-Supported Lipid Bilayers Formed by Langmuir−Blodgett deposition: a tutorial. *Langmuir* **2018**, *34*, 15622−15639.

(31) Brzoska, J. B.; Azouz, I. B.; Rondelez, F. Silanization of Solid Substrates: A Step Toward Reproducibility. *Langmuir* **1994**, *10*, No. 4367.

(32) Zhuang, Y.-X.; Hansen, O.; Knieling, T.; Wang, C.; Rom-bach, P.; Lang, W.; Benecke, W.; Kehlenbeck, M.; Koblitz, J. Thermal

stability of vapor phase deposited self-assembled monolayers for MEMS anti-stiction. *J. Micromech. Microeng.* **2006**, *16*, No. 2259.
(33) Guan, D. S.; Wang, Y. J.; Charlaix, E.; Tong, P. Simultaneous observation of asymmetric speed-dependent capillary force hysteresis and slow relaxation of a suddenly stopped moving contact line. *Phys. Rev. E* **2016**, *94*, No. 042802.
(34) Di Meglio, J.-M.; Quéré, D. Contact Angle Hysteresis: a First Analysis of the Noise of the Creeping Motion of the Contact Line. *Europhys. Lett.* **1990**, *11*, No. 163.
(35) Krafft, M. P.; Riess, J. G. Chemistry, Physical Chemistry, and Uses of Molecular Fluorocarbon-Hydrocarbon Diblocks, Triblocks, and Related Compounds-Unique "Apolar" Components for Self-Assembled Colloid and Interface Engineering. *Chem. Rev.* **2009**, *109*, No. 1714.
(36) Dalvi, V. H.; Rossky, P. J. Molecular origins of fluorocarbon hydrophobicity. *Proc. Natl. Acad. Sci. U.S.A.* **2010**, *107*, No. 13603.
(37) Israelachvili, J. N. *Intermolecular and Surface Forces*, 3rd ed.; Academic Press, 2011; p 93.

https://doi.org/10.1021/acs.langmuir.1c00079
Langmuir 2021, 37, 4879−4890